EARTHQUAKE ENGINEERING AND STRUCTURAL DYNAMICS
Earthquake Engng. Struct. Dyn. **27**, 917–936 (1998)

NON-LINEAR DYNAMIC EARTH DAM–FOUNDATION INTERACTION USING A BE–FE METHOD

HASSAN ABOUSEEDA† AND PANOS DAKOULAS*,‡
Civil Engineering Department, MS 318, Rice University, 6100 Main Street, Houston, TX 77005-1892, U.S.A.

SUMMARY

A general, rigorous, coupled Boundary Element–Finite Element (BE–FE) formulation is presented for non-linear seismic soil–structure interaction in two dimensions. The BE–FE method is applied to investigate the inelastic response of earth dams to transient SV waves. The dam body, consisting of heterogeneous materials modelled with a simple non-linear hysteretic model, is discretized with finite elements, whereas the elastic half-space is discretized with boundary elements. The study focuses on the combined effects of the material non-linearity and foundation flexibility. The results show the significant effect of the foundation flexibility in reducing the response through radiation of energy. For excitations with peak ground accelerations from 0·2*g* to 0·6*g*, the crest acceleration amplification ranges from 2·5 to 1·4 and seems to be comparable with field observations and results from other studies. Deamplification increasing with strain is reported at the lower part of the dam. The method is computationally powerful and can be used for efficient non-linear analysis of complex soil–structure systems. The efficiency of the BE–FE method allows further improvements with incorporation of a more advanced constitutive model and consideration of the generation and dissipation of pore-water pressures during the earthquake. © 1998 John Wiley & Sons, Ltd.

KEY WORDS: earth dams; soil–structure interaction; non-linear analysis; seismic response; boundary elements; finite elements

INTRODUCTION

Earth and rockfill dams built in seismic regions, must be designed safely and economically to withstand potentially strong earthquakes. A realistic assessment of the behaviour of such dams to strong ground shaking depends significantly on the proper consideration of factors such as the dam and canyon geometry, the inhomogeneity and the non-linear inelastic behaviour of the material, the relative flexibility of the dam and canyon (or foundation) materials and the spatial variability of the excitation.[1–12] Detailed accounts of past contributions are available in two state-of-art reports by Gazetas[14] and Gazetas and Dakoulas.[15]

Dam–foundation interaction

A series of studies have shown that the effects of the spatial variability of the ground motion and the flexibility of the foundation or canyon material are significant and should be taken into account.[1,3,6–10] Recently, Dakoulas and his co-workers[7–10] presented a series of closed-form solutions for dams built in flexible canyons of semicircular, semielliptical and rectangular shapes and subjected to obliquely incident SH

* Correspondence to: Panos Dakonlas, Civil Engineering Department, MS 318, Rice University, 6100 Main Street, Houston, TX 77005-1892, U.S.A. E-mail: dakoulas@rice.edu
† Former Graduate Student
‡ Associate Professor

CCC 0098–8847/98/090917–20$17·50

Received 18 June 1996
Revised 4 September 1997 and 21 January 1998

waves. Moreover, using a frequency-domain BE–FE formulation, the authors pressented studies[1,6] for plane-strain dams subjected to P, SV and Rayleigh waves. These theoretical and numerical solutions account rigorously for the dam–canyon interaction and the wave scattering and diffraction phenomena associated with the presence of the dam. The results from all studies demonstrate that the spatial variability of the ground motion induces new vibrational modes which may lead to substantially higher response in the dam than that caused by spatially invariant motion. The amount of energy radiated back into the canyon depends on the impedance ratio, $IR = V_f \rho_f / V_d \rho_d$, where V_f, V_d are the S-wave velocities and ρ_f, ρ_d are the mass densities of the foundation and dam materials, respectively. The radiation damping may reduce substantially the dam response, compared to that for rigid base. Given the importance of the base flexibility and the spatial variability of the ground motion, it is essential to account for their effects during seismic evaluations of embankment dams.

Non-linear inelastic behaviour

Soils under large strains exhibit a complex and highly non-linear behaviour, which may affect substantially the seismic behaviour of embankment dams. In current seismic evaluations, satisfactory seismic performance means that the anticipated permanent deformations for the design earthquake remain within certain acceptable limits.[19] Thus, whenever the factor of safety is low, a more detailed analyses may be warranted to ensure that the anticipated permanent deformation is acceptable. Despite significant progress, prediction of realistic permanent deformations for the design earthquake is still an unresolved problem. Over the last three decades, the most common approach to computing rough estimates of permanent deformations has been Newmark's sliding-blick concept.[18,19] This simplified procedure assumes that all permanent deformation occurs only along the slip surface and that the computation of the dam response and the slip can be performed in two uncoupled steps. Notwithstanding the usefulness of the sliding-block method in offering an index of potential deformation for preliminary evaluation, it cannot provide the actual permanent deformation patterns required in detailed seismic evaluations.[13] A recent coupled single-step approach offers a significant improvement of the method.[16]

A more rigorous treatment of soil inelastic behaviour under cyclic load is through elastoplastic constitutive models based on kinematic hardening.[11,12,22,23] In this, a hardening law expresses the change of the plastic modulus by using multi-yield or boundary surface theory. The method has been extended considering the soil as a two-phase medium with fully coupled soil skeleton and pore-water pressure developing in the saturated portion of the dam.[24] Such elastoplastic constitutive models in coupled formulations require substantial computation times.[13,15]

An efficient alternative is the use of direct modelling of the non-linear stress–strain behaviour of soil.[13,25,26] Finn *et al.*[26] developed an approximate model based on a hyperbolic stress–strain relationship with Masing criterion to represent the cyclic behaviour in simple shear. Incorporated in a 2-D FE formulation, the model considers transient and residual pore-water pressure generated and diffused during the shaking, and volumetric comparison due to shear. Comparisons with published data for embankment dams and centrifuge tests have shown that the model provides good engineering accuracy. This cost-effective approach has been used successfully for more than a decade by the U.S. Army Corps of Engineers for dynamic effective-stress large-deformation analyses of embankment dams.[13,23]

Finally, generalized plasticity models are becoming increasingly more popular, as they allow a more convenient framework of plasticity theory that does not require explicit definition of the yield and plastic potential surfaces or application of the consistency condition. Such models seem to provide efficient and reasonably accurate predictions for static and dynamic loading conditions, and have been used successfully in large-deformation analyses of embankment dams and centrifuge tests.[27]

It should be noted that, due to heavy computation times, the aforementioned non-linear formulations either ignore entirely the effects of dam–foundation interaction or approximate the radiation of energy with simple absorbing elements.

Methods of analysis

Due to inherent limitations, standard numerical techniques for dynamic analysis of soil–structure systems are not perfectly suited for considering adequately essential factors controlling the dam response. While FE methods are ideal for complex geometries and material inhomogeneity and non-linearity in finite domains, they are less efficient and accurate with infinite domains due to wave reflection at artificial boundaries. A variety of formulations and element types were devised to handle such problems, including infinite elements.[28–32] On the other hand, boundary-type methods are superior in handling infinite domains,[33] but they are better suited for linear problems, without significantly enlarging the computational effort using subdomain techniques.[34]

To benefit from the advantages and avoid the limitations of the two methods, Zienkiewicz *et al.* introduced a hybrid BE–FE method for problems of complex geometry, and material heterogeneity and non-linearity in the near field.[33,35–37] In the time domain, the coupled BE–FE method was used to study the transient response of flexible 2-D and 3-D foundations subjected to external dynamic forces and seismic waves,[28,38] and the response of a force-excited layered half-space and a wave-excited 2-D trench.[39] Von Estorff and Kausel[37] applied the technique on various soil–structure interaction problems such as flexible foundations, trenches and tunnels, whereas Touhei and Ohmachi[40,41] studied the linear dynamic interaction of the dam, foundation and reservoir.

The first inelastic formulation of the dynamic coupled FE–BE method was published by Pavlatos and Beskos.[42] Applications of the technique have been presented recently by Pavlatos and Beskos[43] and Valliappan and Yazdchi.[44] In the following, a general, rigorous, cost-effective coupled FE–BE formulation is presented for non-linear dynamic soil–structure interaction and used to investigate the seismic behaviour of earth dams.

NON-LINEAR COUPLED FE–BE FORMULATION

The dynamic soil–structure interaction model assumes that the dam and possibly a foundation soil layer (near field) may behave non-linearly, whereas the rest of the half-space (far field) behaves as a linear elastic material (Figure 1). The far-field region, Ω^{B}, is discretized using BE into a set of nodes consisting of the outer nodes Γ_{o}^{B} and the interface nodes Γ_{i}^{B}. Similarly, the near-field region, Ω^{F}, is discretized using FE into another set of nodes consisting of the interface nodes Γ_{i}^{F} and the remaining nodes Γ_{r}^{F}.

Boundary integral formulation

For zero initial conditions and body forces, Love's integral representation becomes[45]

$$c_{ij}u_i(\xi, t) = \int_{\Gamma} \{(G_{ij} \otimes t_i)(x, t) - (F_{ij} \otimes u_i)(x, t)\}\, d\Gamma \tag{1}$$

where $u_i(x, t)$ and $t_i(x, t)$ are the displacement and traction components i at point x and time t, $G_{ij} = G_{ij}(x, t, \xi, \tau)$ and $F_{ij} = F_{ij}(x, t, \xi, \tau)$ are the displacement and traction components i at point x due to

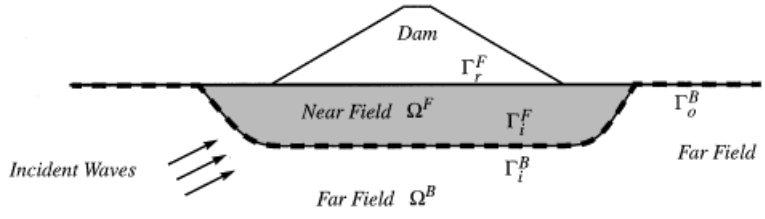

Figure 1. Earth dam, foundation layer (near field) and elastic half-space (far field)

a concentrated pulse in direction j at point ξ in a homogeneous linear elastic solid of infinite extent (see the appendix), the symbol $\otimes$ indicates convolution in time, and c_{ij} for smooth boundaries is equal to δ_{ij} if $\xi \in \Omega^{\mathrm{B}}$ and $0.5\delta_{ij}$ if $\xi \in \Omega^{\Gamma}$.

The solution of equation (1) requires approximation of the temporal and spatial variation of $u_i(x, t)$ and $t_i(x, t)$, which are assumed constant within each time step Δt. At time step N, equation (1) is written as

$$c_{ij}u_i^N(\xi, t) = \sum_{n=1}^{N} \int_{\Gamma} \{G_{ij}^n(x, t, \xi, \tau)t_i^{N-n+1}(x) - F_{ij}^n(x, t, \xi, \tau)u_i^{N-n+1}(x)\}\, \mathrm{d}\Gamma \tag{2}$$

where $\{u^N\}$ and $\{t^N\}$ are the displacement and traction vectors for all boundary nodes, G_{ij}^n and F_{ij}^n are the temporal integrals of the fundamental solutions G_{ij} nad F_{ij} at time step n, given by

$$G_{ij}^n(x, t, \xi, \tau) = \int_{(n-1)\Delta t}^{n\Delta t} G_{ij}(x, 1, \xi, \tau)\, \mathrm{d}\tau \tag{3}$$

and

$$F_{ij}^n(x, t, \xi, \tau) = \int_{(n-1)\Delta t}^{n\Delta t} F_{ij}(x, t, \xi, \tau)\, \mathrm{d}\tau \tag{4}$$

The boundary is modelled using isoparametric linear elements, for which the co-ordinates, displacements and tractions are computed by $x_i = \sum_k N_k^B(\zeta)X_{ik}$, where X_{ik} are the nodal values and N^{B} is the shape function with co-ordinate ζ. Thus, equation (2) becomes

$$c_{ij}u_i^k(\xi, t) = \sum_{n=1}^{N} \sum_{m=1}^{M} \left[\sum_k T_{ik}^{N-n+1} \int_{-1}^{1} G_{ij}^n(x, t, \xi, \tau)N_k^{\mathrm{B}}(\zeta)|J|\, \mathrm{d}\zeta \right.$$
$$\left. - U_{ik}^{N-n+1} \int_{-1}^{1} F_{ij}^n(x, t, \xi, \tau)N_k^{\mathrm{B}}(\zeta, \eta)|J|\, \mathrm{d}\zeta \right] \tag{5}$$

where U_{ik}^N, T_{ik}^N are the nodal displacements and tractions, M is the number of BE and $|J|$ is the Jacobian of element transformation. After integration, equation (5) is expressed as

$$[F^1]\{u^N\} = [G^1]\{t^N\} + \sum_{n=2}^{N} ([G^n]\{t^{N-n+1}\} - [F^n]\{u^{N-n+1}\}) \tag{6}$$

where $[G^n]$ and $[F^n]$ are the coefficient matrices of the system at time $n\Delta t$. For the current time step N, all traction vectors $\{t^n\}$, $n = 1$ to N, and previous displacement vectors $\{u^n\}$, $n = 1$ to $N - 1$, are known.

Boundary truncation at a certain distance from the structure has given very good results.[1,2,6]

Finite element formulation

The co-ordinates, displacements and tractions within each FE are approximated by $x_i = \sum_k N_k^F(\zeta, \eta)X_{ik}$, where X_{ik} are the nodal values and N^{F} is the shape function of a standard element with coordinates (ζ, η). The Galerkin weighted residual formulation is used, with a weighting function identical to the shape function. This discretization yields the equation

$$[M]\{\ddot{u}^N\} + [C^{N-1}]\{u^N\} + \{p^N\} + \{f^N\} = 0 \tag{7}$$

where $\{u^N\}$, $\{p^N\}$ and $\{f^N\}$ are the displacement, internal force and applied force vectors at time step N; $[M]$ and $[C^N]$ are the global mass and damping matrices. The internal force vector is given by

$$\{p^N\} = \{p^{N-1}\} + [K_T^{N-1}]\{\Delta u^N\} \tag{8}$$

in which

$$\{\Delta u^N\} = \{u^N\} - \{u^{N-1}\} \tag{9}$$

and $[K_T^N]$ is the tangent stiffness matrix. The individual element matrices and vectors are

$$M^e = \int_{\Omega^e} N^T \rho N \, d\Omega, [K_T^e] = \int_{\Omega^e} B^T D_{ep} B \, d\Omega, f^e = -\int_{\Omega^e} N^T b \, d\Omega + \int_{\Omega^e} B^T \sigma \, d\Omega \tag{10}$$

where B is the strain shape function, D_{ep} the elastoplastic matrix, b the body force per unit volume and σ the applied stress. The damping matrix is expressed as $[C^N] = (\alpha_m[M] + \alpha_k[K^N])$ where α_m, α_k are the mass and stiffness damping factors respectively. The integrations are evaluated using the Gauss quadrature. The time integration is carried out by the Newmark β scheme, which approximates the displacement derivatives at time step N from the displacement and its derivatives at time step $N-1$. The velocities and accelerations are given by

$$\{\dot{u}^N\} = \frac{\theta}{\beta \Delta t}[\{u^N\} - \{u^{N-1}\}] + \left(1 - \frac{\theta}{\beta}\right)\{\dot{u}^{N-1}\} + \left(1 - \frac{\theta}{2\beta}\right)\Delta t\{\ddot{u}^{N-1}\} \tag{11}$$

$$\{\ddot{u}^N\} = \frac{1}{\Delta t^2 \beta}[\{u^N\} - \{u^{N-1}\}] + \frac{\beta}{\Delta t}\{\dot{u}^{N-1}\} + \left(1 - \frac{\theta}{2\beta}\right)\{\ddot{u}^{N-1}\} \tag{12}$$

where $\beta \geqslant 0{\cdot}25$ and $\theta \geqslant 0{\cdot}5$. The solution of the system is achieved by using an iterative Newton–Raphson scheme at every time step. The system matrices are computed at each time step.

Coupling of boundary and finite elements

Equation (6) can now be written as

$$\{t^N\} = [V^1]\{u^N\} + \sum_{n=2}^{N} ([W^n]\{t^{N-n+1}\} - [V^n]\{u^{N-n+1}\}) \tag{13}$$

where $[V^n] = [G^1]^{-1}[F^n]$ and $[W^n] = [G^1]^{-1}[G^n]$. Equation (13) can be further modified as

$$\begin{bmatrix} t_i^N \\ t_o^N \end{bmatrix} = \begin{bmatrix} V_{ii}^1 & V_{io}^1 \\ V_{oi}^1 & V_{oo}^1 \end{bmatrix}\begin{bmatrix} u_i^N \\ u_o^N \end{bmatrix} + \sum_{n=2}^{N}\left\{\begin{bmatrix} W_{ii}^n & W_{io}^n \\ W_{oi}^n & W_{oo}^n \end{bmatrix}\begin{bmatrix} t_i^{N-n+1} \\ t_o^{N-n+1} \end{bmatrix} - \begin{bmatrix} V_{ii}^n & V_{io}^n \\ V_{oi}^n & V_{oo}^n \end{bmatrix}\begin{bmatrix} u_i^{N-n+1} \\ u_o^{N-n+1} \end{bmatrix}\right\} \tag{14}$$

where the i subscript denotes the interface nodes and the o subscript denotes the outer nodes. Equation (14) represents the traction vectors t_i^N and t_o^N as a function of the displacement vectors u_i^N and u_o^N. By eliminating u_o^N, one can write the following expression:

$$\{t_i^N\} = [K_{ii}^B]\{u_i^N\} + \{R\} \tag{15}$$

where

$$[K_{ii}^B] = [V_{ii}^1] - [Y][V_{oi}^1] \tag{16}$$

$$[Y] = [V_{io}^1][V_{oo}^1]^{-1} \tag{17}$$

$$\{R\} = [Y][t_o^N] + \sum_{n=2}^{N}\begin{pmatrix} [V_I^n]\{u_i^{N-n+1}\} + [V_{II}^n]\{u_o^{N-n+1}\} \\ -[W_I^n]\{t_i^{N-n+1}\} - [W_{II}^n]\{t_o^{N-n+1}\} \end{pmatrix} \tag{18}$$

$$[V_I^n] = [V_{ii}^n] - [Y][V_{oi}^n] \tag{19}$$

$$[V_{\mathrm{ii}}^{n}] = [V_{\mathrm{io}}^{n}] - [Y][V_{\mathrm{oo}}^{n}] \tag{20}$$

$$[W_{\mathrm{i}}^{n}] = [W_{\mathrm{ii}}^{n}] - [Y][W_{\mathrm{oi}}^{n}] \tag{21}$$

$$[W_{\mathrm{ii}}^{n}] = [W_{\mathrm{io}}^{n}] - [Y][W_{\mathrm{oo}}^{n}] \tag{22}$$

Since the tractions on the outer surface are known, $\{R\}$ is also known and equation (15) can be used to compute the $\{u_{\mathrm{i}}^{N}\}$ and $\{t_{\mathrm{i}}^{N}\}$ at the interface nodes $\Gamma_{\mathrm{i}}^{\mathrm{B}}$. Similarly, the FE subregion nodes are divided in the interface nodes $\Gamma_{\mathrm{i}}^{\mathrm{F}}$ and the remaining nodes $\Gamma_{\mathrm{r}}^{\mathrm{F}}$. Equation (7) can be written as

$$\begin{bmatrix} K_{\mathrm{rr}}^{\mathrm{F}} & K_{\mathrm{ri}}^{\mathrm{F}} \\ K_{\mathrm{ir}}^{\mathrm{F}} & K_{\mathrm{ii}}^{\mathrm{F}} \end{bmatrix} \begin{bmatrix} u_{\mathrm{r}}^{N} \\ u_{\mathrm{i}}^{N} \end{bmatrix} + \begin{bmatrix} f_{\mathrm{r}} \\ f_{\mathrm{i}} \end{bmatrix} = \{0\} \tag{23}$$

Note that $\{t\}$ represesnts the tractions along the boundary, whereas $\{f\}$ represents the forces at the nodes. By expressing the BE tractions as a function of nodal values

$$t^{N} = [N^{\mathrm{B}}]^{\mathrm{T}}\{t_{\mathrm{i}}^{N}\} \tag{24}$$

the nodal forces are computed using the transformation matrix $A = \int_{\Gamma_{\mathrm{i}}} [N^{\mathrm{F}}]^{\mathrm{T}}[N^{\mathrm{B}}]\,\mathrm{d}\Gamma_{\mathrm{i}}$. From equations (15) and (23), the following system is obtained:

$$\begin{bmatrix} K_{\mathrm{rr}}^{\mathrm{F}} & K_{\mathrm{ri}}^{\mathrm{F}} & 0 \\ K_{\mathrm{ir}}^{\mathrm{F}} & K_{\mathrm{ii}}^{\mathrm{F}} & A \\ 0 & K_{\mathrm{ii}}^{\mathrm{B}} & I \end{bmatrix} \begin{bmatrix} u_{\mathrm{r}}^{N} \\ u_{\mathrm{i}}^{N} \\ t_{\mathrm{i}}^{N} \end{bmatrix} = \begin{bmatrix} -f_{\mathrm{r}} \\ -f_{\mathrm{i}} \\ R \end{bmatrix} \tag{25}$$

which is solved for the displacements u_{r}^{N}, u_{i}^{N} and the tractions t_{i}^{N} at the time step N. Once these values are known, the displacements at the outer nodes of the BE subregion $\Gamma_{\mathrm{o}}^{\mathrm{B}}$ can be computed. Further condensation of equation (25) can be achieved, if only the near-field response is of interest.

Non-linear stress–strain model

The above general BE–FE formulation can be combined with any rigorous elastoplastic model for non-linear soil–structure interaction analysis. Although the final formulation will incorporate such a rigorous model, to preserve simplicity at this stage of development, the Ramberg–Osgood model with the Masing criterion is used. This model is analogous to the hyperbolic model by Finn *et al.*[13,25,26] For the vertically incident SV waves considered in the application pressented here, the dam responds mainly in shear vibration. Figure 2 ilustrates the shear stress–shear strain relationship (τ–γ) of the Ramberg–Osgood model, defined by

$$\frac{\gamma}{\gamma_{\mathrm{y}}} = \frac{\tau}{\tau_{\mathrm{y}}} + \alpha \left| \frac{\tau}{\tau_{\mathrm{y}}} \right|^{r} \quad \text{for virgin loading} \tag{26}$$

and

$$\frac{\gamma - \gamma_0}{2\gamma_{\mathrm{y}}} = \frac{\tau - \tau_0}{2\tau_{\mathrm{y}}} + \alpha \left| \frac{\tau - \tau_0}{2\tau_{\mathrm{y}}} \right|^{r} \quad \text{for unloading/reloading} \tag{27}$$

where γ_{y} and τ_{y} are nominal 'yielding' strain and stress, respectively, and α, r are material constants. For the vertically incident SV waves considered, it is reasonable to consider that $\tau = \tau_{xz}$ and $\gamma = \gamma_{xz}$.[25,26] The values for the model parameters α, r, γ_{y} and τ_{y} must yield results that agree with available experimental data on cyclic behaviour of the materials involved. To this end, the following criteria were satisfied in choosing these parameters: (a) the reduction of the secant shear modulus G/G_0 is taken equal to 0·9 at strain $\gamma = \gamma_{\mathrm{y}}$

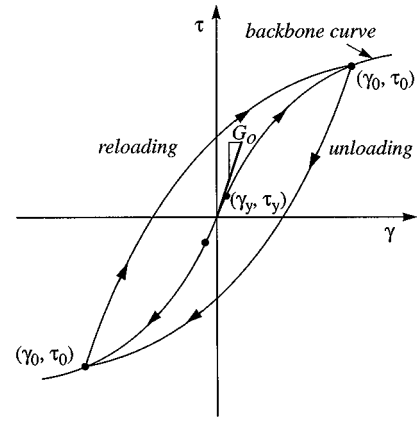

Figure 2. The Ramberg–Osgood model for loading, unloading and reloading

(approximately elastic range); (b) a very good agreement of the G/G_0 and β at any level of cyclic shear strain is enforced between the Ramberg–Osgood model predictions and the experimental data for gravel and sand; (c) The maximum shear strength is attained at a desirable strain, which in this study is taken equal to 2 per cent.

Input motion

Figure 3(a) represents a typical soil–structure system, subjected to seismic waves propagating from the far field to the near field. A horizontal wave input boundary Γ is defined within the far field as shown in Figure 3(b). First, the wave boundary Γ is artificially fixed, so that the incident wave reflects inducing reaction stresses σ_Γ on Γ, whereas no motion is transmitted above Γ. Then, by introducing the opposite of σ_Γ at Γ (Figure 3(c)), the effect of the fixed boundary is eliminated. In most cases, the engineer is interested in the response of the structure and the near field, which is given solely by the analysis represented in Figure 3(c). Because there is no contribution in the response of the structure and near field from case (b), no superposition is needed and therefore the non-linearity of the structure and near field poses no problem. For the rare case of evaluation of the response below the wave input boundary Γ, a superposition of the linear response of the far-field domain from cases b and c should be obtained. Thus, the problem in Figure 3(a) is equivalent to solving the two problems in Figure (3b) and 3(c). A detailed general treatment of the input excitation formulation has been already published in the literaure.[31,32] For the applications considered in this study, Γ is taken at the surface of the half-space.

Numerical implementation and solution behaviour

The numerical implementation of the formulation uses a Newmark β scheme to approximate the displacement derivatives.[46] Higher values of the factor β result to increased stability of the solution. Values of $\gamma \geqslant 0{\cdot}7$ and $\beta = 0{\cdot}5$ are used in the following parametric studies, where γ and β are defined in Reference 46.

To ensure the numerical stability of the hybrid formulation, two additional measures were employed: (a) In the FE domain, in addition to the hysteretic damping provided by the non-linear stress–strain behaviour of the soil, a small amount (1 per cent) of mass and stiffness proportional damping was introduced. (b) Similarly, in the BE domain, a small amount of numerical, stiffness-proportional damping was introduced by adding a new term in equation (15), which is rewritten as

$$\{t_i^N\} = [K_{ii}^B]\{u_i^N\} + \beta_b[K_{ii}^B]\{\dot{u}_i^N\} + \{R\} \tag{28}$$

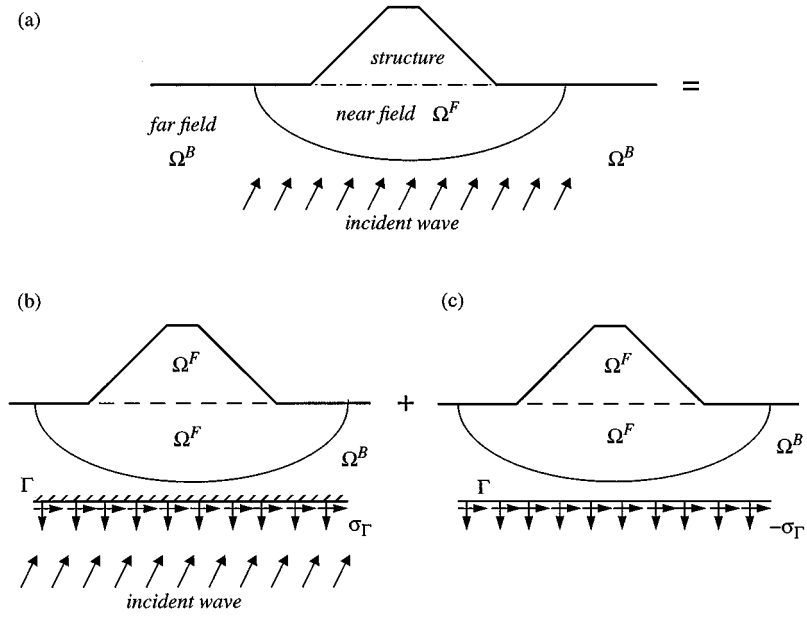

Figure 3. Wave input model for an infinite medium

where β_b is a Rayleigh-type stiffness proportional damping factor. This factor is important in ensuring the stability of the numerical solution. A very small value of $\beta_b = 0{\cdot}001$ yielded a well-behaved solution, without having any adverse effect on the response values.

To account for the use of constant values of displacements and tractions throughout the time step Δt, small time increments were used. Such small values of Δt also contribute to a better representation of the non-linear behaviour of the model. A time step of $\Delta t = 0{\cdot}004$ s was used in the following examples. Solving the system of equations and backtracking displacement and traction histories are the most time-consuming tasks of the numerical solution. Shorter computational times can be achieved by limiting the backtracking procedure to a certain number of time steps, N_{limit}. In this case, the summations in (6) and (18) should be from 2 to N_{limit}, for $N \leqslant N_{\text{limit}}$. Numerical results show that this procedure has almost no effect on the response values, given that N_{limit} is large enough so that $F_{ij}^{n=N_{\text{limit}}}$ and $G_{ij}^{n=N_{\text{limit}}}$ have decreased to < 5 per cent of their peak value. The computation time for 3750 steps using a personal computer is about 2.5 h.

Verification of time-domain BE–FE formulation

The developed algorithm of the coupled BE–FE formulation was verified in a systematic step-by-step way. First, the coupled time-domain BE–FE was verified for linear analysis, by comparing the results with published results from benchmark problems. To this end, the response of a linear elastic half-space subjected to an instantaneous surface stress increment is considered, as shown in Figure 4. Results for this problem have been given by Antes,[47] Cruse and Rizzo[48] and Mansur *et al.*[49] A vertical impulse stress $q = 68.95$ MPa acts on a strip of width $2b = 152{\cdot}4$ m. The elastic half-space has a Young's modulus $E = 17240$ MPa, density $\rho = 3150$ kg/m^3 and Poisson's ratio $\nu = 0{\cdot}25$. Figure 4 plots the vertical responses evaluated at points A, B and C. The results demonstrate clearly that the response obtained by the coupled FE–BE formulation is in good agreement with the published rigorous BE solutions at all points. The responses of a flexible strip-footing on elastic half-space subjected to a concentrated load derived from this model and from a linear hybrid FE–BE formulation by Sprakos and Beskos[38] found in good agreement (the results are not shown

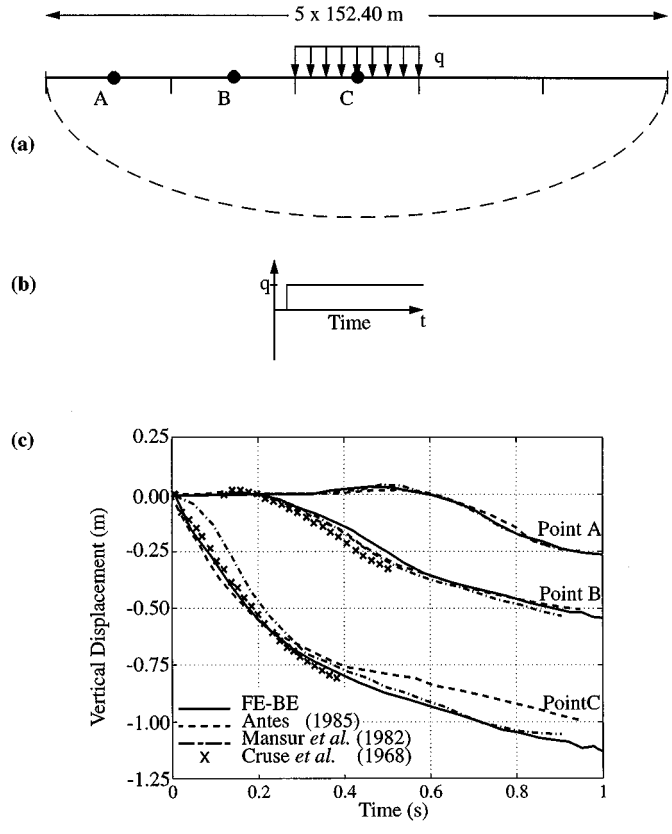

Figure 4. (a) Spatial discretization of the half-space under discontinuous boundary stress distribution. (b) Time history of applied stress. (c) Vertical displacements at the boundary points

due to lack of space). Moreover, the validity of the linear FE formulation was confirmed by comparing the results with those from a general-purpose FE program.[50] Finally, the validity of the non-linear behaviour of the FE formulation was considered by examining the consistency of the results of individual elements with the soil model predictions.

NON-LINEAR RESPONSE OF A DAM–FOUNDATION SYSTEM

Dam–foundation model

The general formulation presented above is now applied to examine the effects of the soil non-linearity and soil–structure interaction on the response of an infinitely long inhomogeneous earth dam. The dam has a height $H = 100$ m, crest width equal to 10 m and symmetric slopes 2 : 1 (Figure 5(a)). The dam material has an average initial shear wave velocity $c_d = 400$ m/s, density $\rho_d = 2000$ kg/m^3, and Poission's ratio $v_d = 1/3$. Stress-dependent elastic moduli and shear strength are considered for the dam body, which is divided into five zones, each having a constant value of elastic modulus and shear strength, as shown in Figure 5(b) A summary of the material properties in each zone is given in Table I. The shear modulus at very small strains G_0 in each zone is estimated using the empirical formula

$$G_0(\text{kPa}) = 1000\, \text{K}_{2,\max}\sqrt{\sigma_0}(\text{kPa}) \tag{29}$$

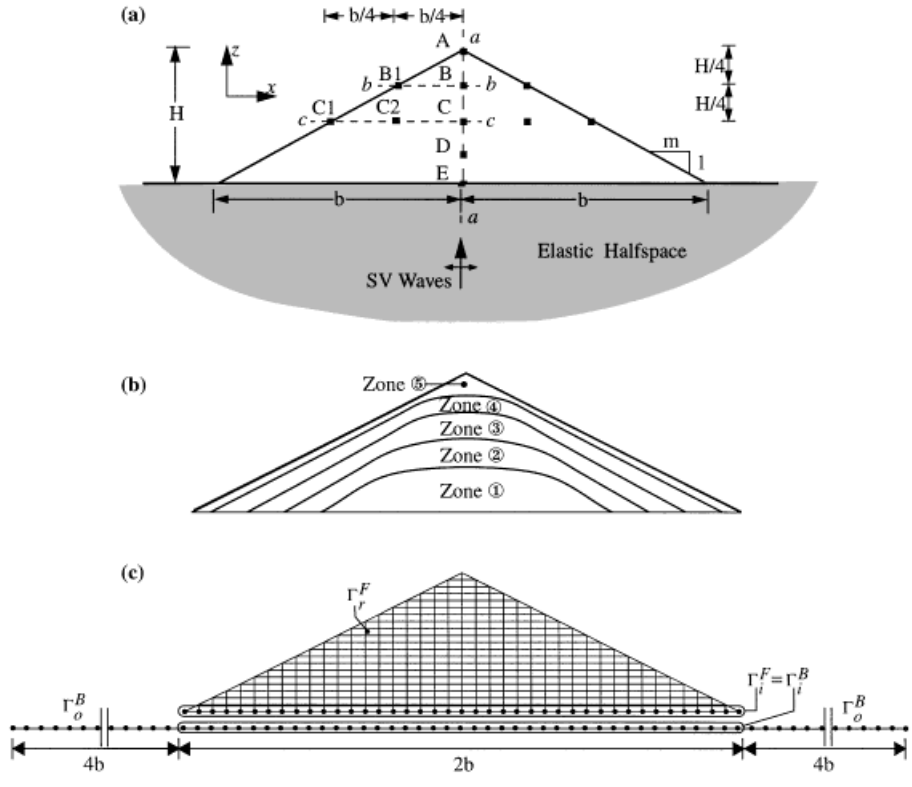

Figure 5. (a) Geometry of the earth dam founded on elastic half-space; (b) different material zones within the dam body; and (c) finite and boundary element meshes

Table I. Material properties in dam zones

Dam zone	E_0 (MPa)	ν	G_0 (MPa)	$\tau_{\max}$ (MPa)	γ_y (%)
1	1150	1/3	430	70	$7{\cdot}8\times10^{-3}$
2	1000	1/3	375	45	$4{\cdot}6\times10^{-3}$
3	850	1/3	319	27	$2{\cdot}6\times10^{-3}$
4	700	1/3	263	17	$1{\cdot}6\times10^{-3}$
5	550	1/3	206	10	$1{\cdot}0\times10^{-3}$

where σ_0 is the average effective confining stress obtained from static analysis and $K_{2,\max} = 35$, corresponding to an average value for very dense sand and gravel (ranging from 30 to 40). For cohesionless gravel and sand material, the maximum shear stress $\tau_{xz,\max}$ is given by

$$\tau_{xz,\max} = \sqrt{\left(\frac{\sigma_z + \sigma_x}{2}\right)^2 \sin^2\phi - \left(\frac{\sigma_z - \sigma_x}{2}\right)^2} - \tau_{xz} \tag{30}$$

where ϕ is the friction angle of dam material. A value of $\phi = 40^\circ$ is used in the current study, corresponding to an average value for very dense sand and gravel. For $\alpha = 0{\cdot}12$ and $r = 2{\cdot}5$, the computed G/G_0 and

β versus cyclic shear strain are in very good agreement with available experimental data for sand and gravel for a wide range of shear strains and confining stresses. These values of α and r are common in all zones, whereas the values of γ_y for each zone are given in Table I. Finally, in addition to the material damping from the hysteretic action of the non-linear model, 1 per cent Rayleigh damping was also included. The foundation material has a shear wave velocity $c_f = 1000$ m/s, density $\rho_f = 2400$ kg/m^3, Poisson's ratio $v_f = 1/3$ and no material damping. The foundation–dam impedence ratio is IR = 3.

The dam body is discretized using 420 four-node plane-strain isoparametric elements, whereas the halfspace is discretized using two-node boundary elements (Figure 5(c)). The discretized length of the half-space surface is taken equal to five times the dam base width.

Input motion

The dam is subjected to a vertically propagating SV wave front resulting to free-field acceleration time history similar to the first 15 s of the El Centro record of the 1940 Imperial Valley Earthquake. The acceleration time history and the Fourier amplitude of the used record are shown in Figure 6. The record was scaled to three different levels of outcrop-rock peak ground acceleration (PGA) equal to 0·2g, 0·4g and 0·6g, to represesnt three levels of non-linearity.

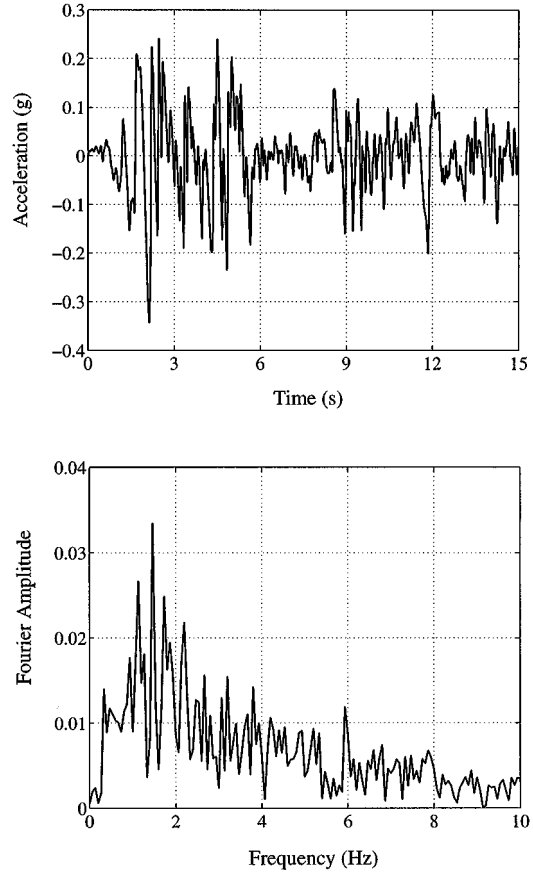

Figure 6. Input Excitation: acceleration time history and Fourier amplitude of the first 15 s of the 1940 Imperial Valley earthquake, El Centro record

Results and discussion

Figure 7 plots the peak values of the horizontal acceleration along the central axis of the dam and across the dam width at elevation $z = 0{\cdot}5H$ and $z = 0{\cdot}75H$, for the three values of PGA = $0{\cdot}2g$, $0{\cdot}4g$ and $0{\cdot}6g$. For comparison, the peak horizontal accelerations along the central axis of the dam and across the dam width are also given for a dam with a rigid base (IR = ∞) in Figure 8.

Notice that for the three levels of PGA the peak crest accelerations are $0{\cdot}89g$, $0{\cdot}72g$ and $0{\cdot}38g$ for IR = 3 and $1{\cdot}2g$, $0{\cdot}88g$ and $0{\cdot}5g$ for the rigid-base dam, respectively. Thus, ignoring the base flexibility overestimates the peak crest acceleration by 35, 22 and 32 per cent, respectively.

Due to radiation of energy back to the half-space, the acceleration at the base is of course smaller for the dam with IR = 3. To evaluate the effect of the material non-linearity on the dynamic response of the dam, it is convenient to compare the amplification $AF_b = \ddot{u}/\ddot{u}_b$, where $\ddot{u}$ = peak acceleration within the dam body and $\ddot{u}_b$ = peak acceleration at the base. On the other hand, to include the effects of foundation flexibility, the standard amplification $AF = \ddot{u}/\ddot{u}_g$ with respect to the outcrop-rock motion will be also considered, where $\ddot{u}_g$ = PGA.

The crest amplifications AF_b of the horizontal acceleration computed from Figure 7 are equal to 2·6, 2·45 and 2·14 for the weakly non-linear, moderately non-linear and strongly non-linear response, respectively. The

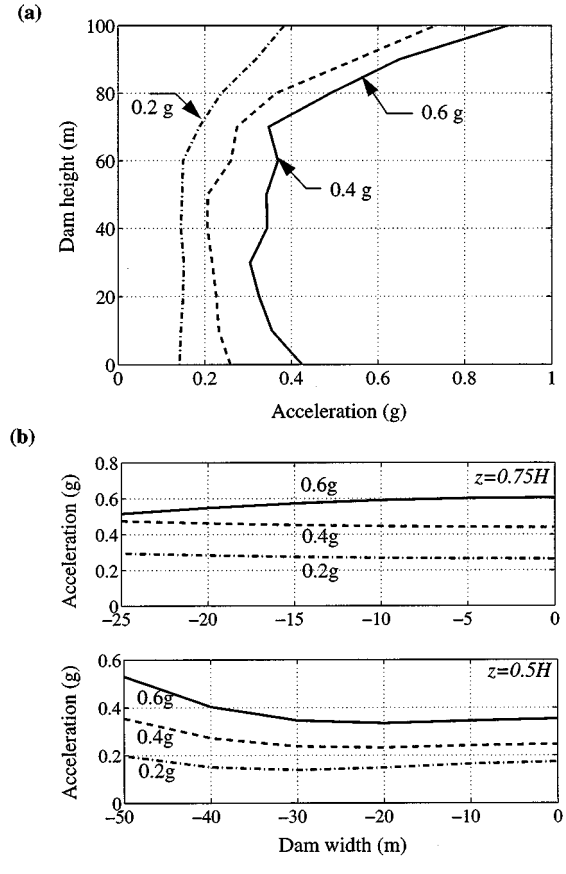

Figure 7. Peak horizontal acceleration for different levels of excitation: (a) along the dam middle axis (section a–a); (b) across the dam half width at $z = 0{\cdot}75H$ (section b–b) and $z = 0{\cdot}5H$ (section c–c). Impedance ratio IR = 3

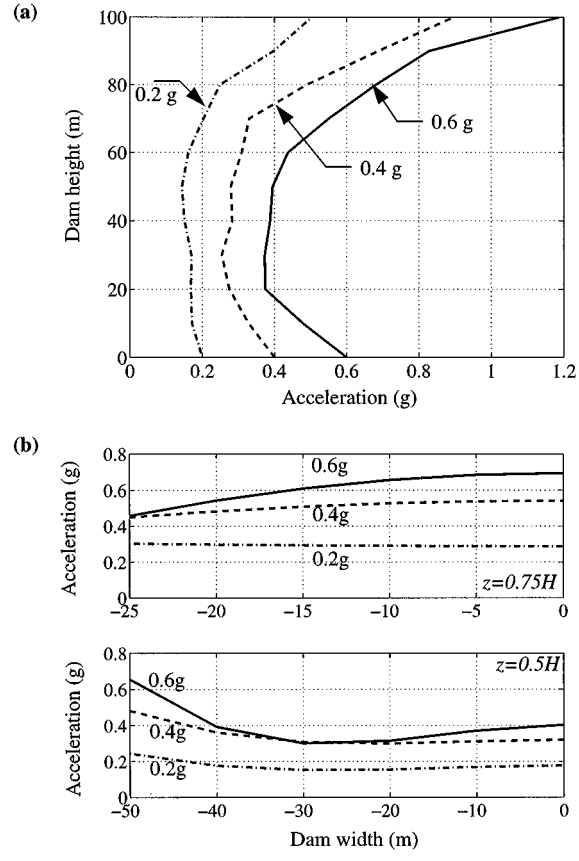

Figure 8. Peak horizontal acceleration for different levels of excitation: (a) along the dam middle axis (section a–a); (b) across the dam half-width at $z = 0{\cdot}75H$ (section b–b) and $z = 0{\cdot}5H$ (section c–c). Impedance ratio IR $= \infty$

corresponding AF_b values for a rigid base dam (Figure 8) are 2·5, 2·2 and 2·0, respectively. For both dams, the acceleration amplification AF_b decreases with increasing level of non-linearity, as the hysteretic damping ratio increases with the amplitudes of cyclic strain. The lower values of AF_b for the rigid-base dam confirm that this dam experiences a higher level of non-linearity compared to the flexible-base dam, in which a portion of the seismic-wave energy is allowed to radiate back into the half-space. For the flexible-base dam, the outcrop-rock amplification AF, including the effect of the foundation flexibility, is 1·9, 1·8, and 1·48, respectively. Comparison of the above AF_b and AF values for the two dams demonstrates that the existence of radiation damping, on the one hand, decreases the dynamic response through energy dissipation into the half-space, and on the other hand, reduces the amount of hysteretic damping, which in itself tends to increase the dynamic response. Moreover, the AF values computed for the flexible base dam seem to be comparable with observed amplifications in actual dams subjected to such earthquake motions.[14,15] For the plane-strain dam and the SV excitation considered, despite its simplicity, the Ramberg–Osgood model yields reasonable results for lateral shear deformation with respect to the general experience from field observations.

Figure 9 plots the horizontal acceleration time history at the points A, B, C, D, E, B1, C1 and C2 (see Figure 5(a)) for the flexible-base dam subjected to PGA = 0·6g. As seismic waves propagate from the base (point E) to the crest (point A), the high-frequency content of the response decreases. Of course, this high-frequency filtering becomes more intense as the level of the earthquake intensity increases, due to higher hysteretic action.

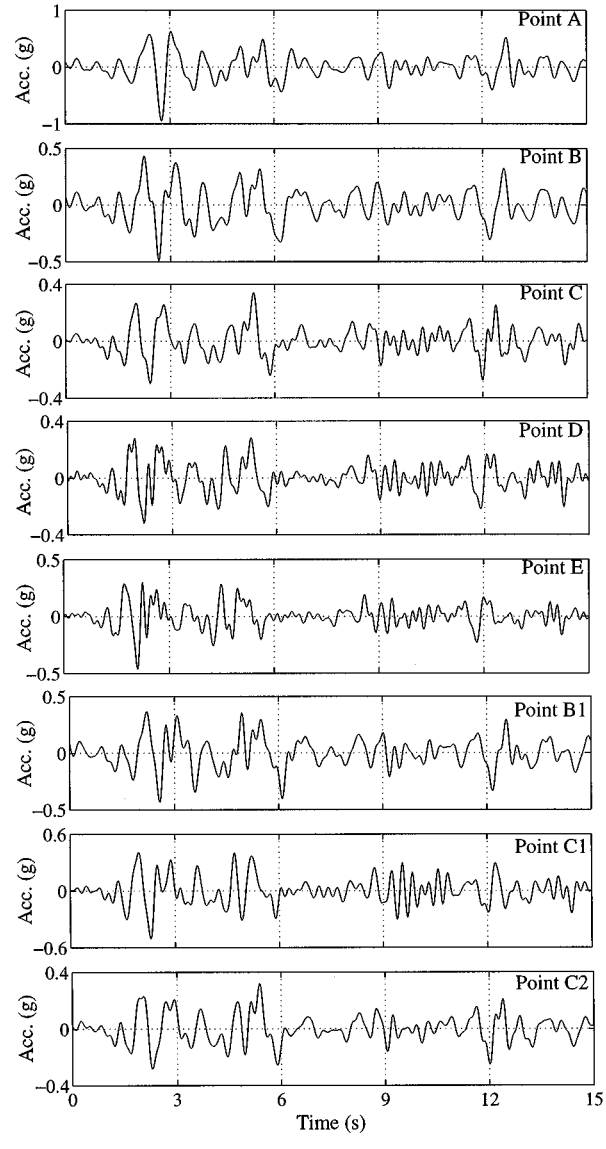

Figure 9. Horizontal acceleration time histories at various points within the dam body for peak ground acceleration = 0·6*g*. Impedance ratio IR = 3

The distribution of the acceleration response along the width of the dam in Figures 7(b) and 8(b) is rather uniform, with some deviation near the slopes of the dam at mid-height, where the response tends to increase due to the higher participation of the high-frequency motion. Indeed, the high-frequency content for point C1 is higher than that for points C2 and B1 (Figure 9), in agreement with the frequency-domain linear analysis.[1] Figures 7(a) and 8(a) show that the acceleration is amplified mainly in the upper quarter and deamplified in the rest of the dam body. The lower acceleration deamplification values are 0·65, 0·5 and 0·49 (flexible-base) and 0·8, 0·68 and 0·61 (rigid-base) for the three levels of excitation, respectively. As expected, this deamplification increases with the intensity of the excitation and the hysteretic action. These results are in agreement with results from other FE studies and field observations where deamplification has been reported.[14,15,23]

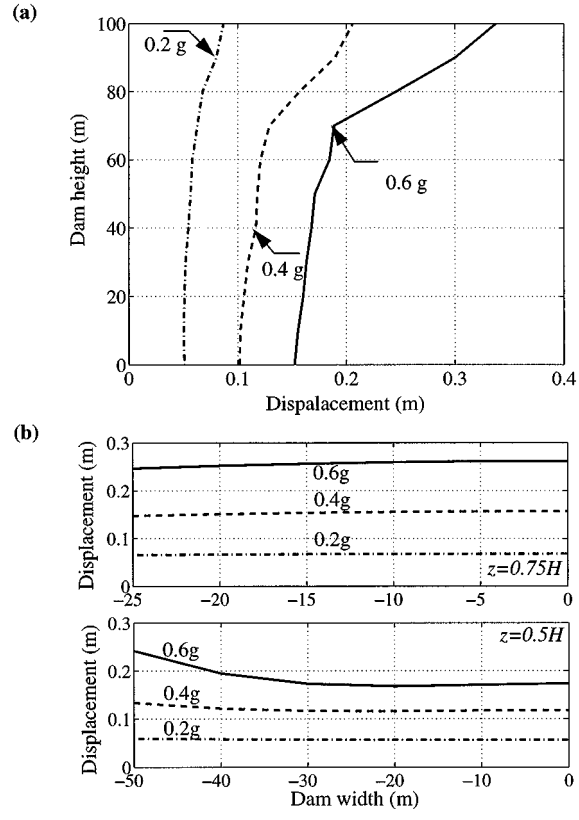

Figure 10. Peak horizontal displacement for different levels of excitation: (a) along the dam middle axis (section a–a); (b) across the dam half width at $z = 0{\cdot}75H$ (section b–b) and $z = 0{\cdot}5H$ (section c–c). Impedance ratio IR = 3

Figure 10 plots the peak displacement response of the flexible-base dam for the three motions considered. The peak crest displacements are 9, 21 and 34 cm for the three motions, respectively; the corresponding peak crest displacements for the rigid-base dam (not shown) are 12, 31 and 36 cm. Again, most of the displacement amplification occurs in the upper quarter of the dam, but there is no displacement deamplification observed in the lower parts of the dam. The difference is due to the fact that displacements depend more on the low-frequency content of the excitation, whereas accelerations on the high-frequency content.

The peak shear strain developed within the dam body is shown in Figure 11. The maximum values occur at a height about $0{\cdot}75H$ and are equal to 0·19, 0·45 and 0·79 per cent, respectively, for the three motions. Figure 11 shows that, as the excitation intensity increases, the upper quarter of the dam body, consisting of material with the smallest stiffness and strength (zones 4 and 5, Table I), experiences the highest level of non-linearly and significant permanent deformation. Figure 12 shows the shear strain time histories and the accumulated permanent shear strain at point B ($z = 0{\cdot}75H$) for the three motions. Note that, although for PGA $= 0{\cdot}2g$ and $0{\cdot}4g$ the peak shear strains occur at the main acceleration pulse ($t \approx 2{\cdot}5$ s), the peak shear strain for PGA $= 0{\cdot}6g$ is affected by the accumulated permanent strain and occurs during a much smaller acceleration pulse ($t \approx 12{\cdot}3$ s). The corresponding peak shear strain developed for the three motions are, respectively, 42, 42 and 50 per cent higher for the rigid-base dam. Figure 13 shows the stress–strain histories and the hysteretic behaviour of the material for the three motions at point B.

The results show that, as the intensity of the excitation increases, the induced level of material nonlinearity affects the accelerations, displacements and strains in different ways, which depend on different ranges of the

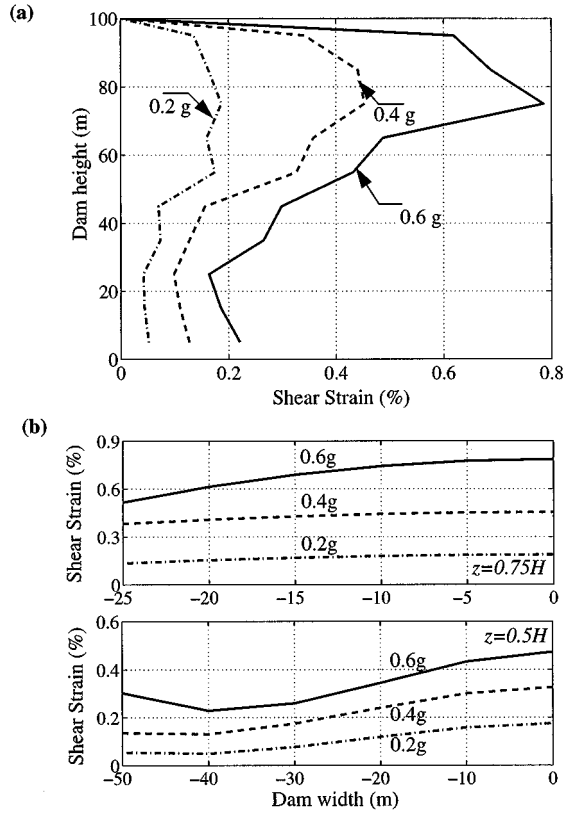

Figure 11. Peak shear strain γ_{zx} for different levels of excitation: (a) along the dam middle axis (section a–a); (b) across the dam half-width at $z = 0{\cdot}75H$ (section b–b) and $z = 0{\cdot}5H$ (section c–c). Impedance ratio IR = 3

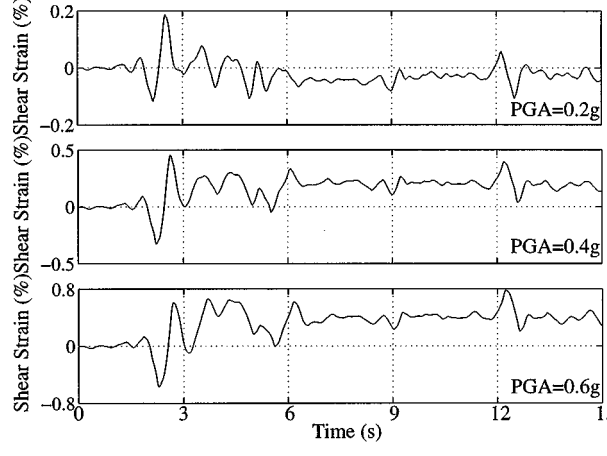

Figure 12. Shear strain time histories for different levels of excitation at point B. Impedance ratio IR = 3

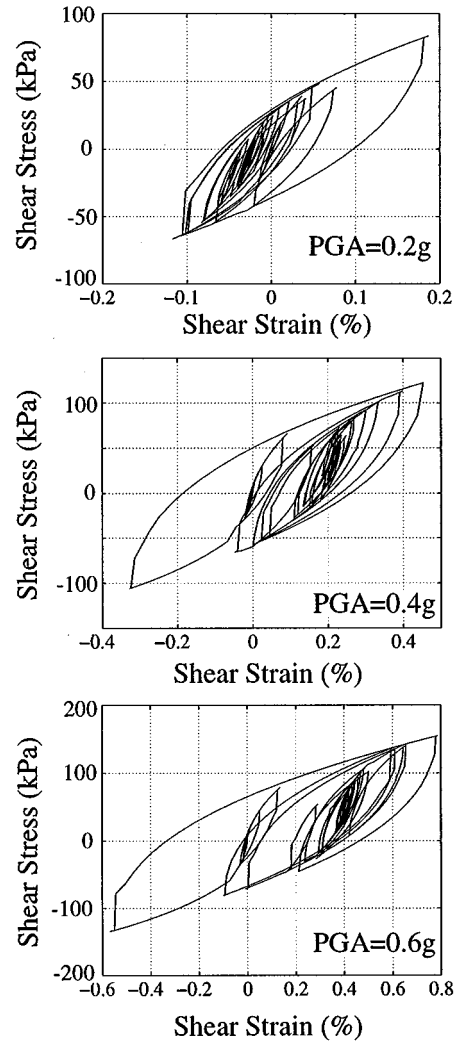

Figure 13. Shear stress versus shear strain at point B($z = 0{\cdot}75H$), for three levels of excitation. Impedance ratio IR = 3

excitation frequency. During high levels of strain and hysteretic damping, the high-frequency content of the transmitted waves is filtered and, as a result, the acceleration amplification within the entire dam body drops. This filtering of the high frequency with increasing nonlinearity is less important for displacements, which are more affected by the decreasing material stiffness, leading to higher values of displacements and strains.

The results demonstrate the ability of the simple nonlinear model to capture the non-linear response, which for SV waves is mainly in shear lateral deformation. The small computational effort needed to account for material non-linearity and soil–structure interaction allows for the application of this formulation to practical engineering problems.

CONCLUSIONS

A general, rigorous, coupled BE–FE formulation was presented for nonlinear seismic soil–structure interaction of 2-D systems. The method can be used to assess the relative importance of non-linearity, soil–structure

interaction, presence of soft foundation layer, spatial variability of excitation and other factors affecting the response of soil–structure systems.

The method was applied here to investigate the response of earth dams to transient vertical SV waves, assuming non-linear hysteretic behaviour for the dam material, with focus on the combined effects of non-linearity and foundation flexibility. The results showed the significant effect of the flexibility of the foundation on dissipating wave energy and reducing the dam response. For the problem considered, ignoring the base flexibility leads to an overestimation of crest accelerations by 35 per cent and of maximum shear strains by 50 per cent. For a flexible base, the resulting smaller non-linearity leads to higher crest-to-base acceleration amplifications than those computed for a rigid base. Thus, some of the beneficial effect of radiation damping is offset by the smaller hysteretic damping. The maximum accelerations occur at the crest and upper quarter of the dam. For excitations with PGA $= 0{\cdot}2g$ to $0{\cdot}6g$, the crest acceleration amplifications were in the range of 2·5 to 1·4 and are comparable with observed amplifications in actual dams subjected to similar levels of earthquake excitations. For the rest of the dam, acceleration deamplification with increasing levels of strain is reported, in agreement with other studies and field observations.[14,15]

The study showed that the presented BE–FE method provides an efficient, rigorous tool for making the formidable task of non-linear seismic soil–structure interaction analysis possible. The efficiency of the model allows for parametric investigations of 2D seismic SSI problems. The incorporation of a more advanced constitutive soil model and consideration of the generation and dissipation of pore water pressures during the earthquake is the next step in improving the usefulness of the model. Such a model could be exceptionally useful for the study of the seismic behaviour of embankment dams, waterfront structures and other soil–structure systems.

APPENDIX. FUNDAMENTAL SOLUTIONS

The fundamental singular solution for displacement component i at point x (receiver) due to a concentrated pulse in direction j at point ξ (source) in an infinite 3-D elastic solid is[45,51,52]

$$G_{ij} = \frac{1}{2\pi\rho r^2}\left\{\frac{1}{c_1}H(c_1t'-r)\left[\left(2R_1+\frac{r^2}{R_1}\right)\left(\frac{r_ir_j}{r^2}\right)-\delta_{ij}R_1\right]\right.$$
$$\left.-\frac{1}{c_2}H(c_2t'-r)\left[\left(2R_2+\frac{r^2}{R_2}\right)\left(\frac{r_ir_j}{r^2}\right)-\delta_{ij}\left(R_2+\frac{r^2}{R_2}\right)\right]\right\} \tag{31}$$

where

$$r_i = x_i - \xi_i \tag{32}$$
$$r = |x_k - \xi_k| \tag{33}$$
$$t' = t - \tau \tag{34}$$
$$c_1 = \sqrt{\frac{\lambda+2\mu}{\rho}} \quad \text{and} \quad c_2 = \sqrt{\frac{\mu}{\rho}} \tag{35}$$
$$R_i = \sqrt{(c_it')^2 - r^2} \quad i = 1, 2 \tag{36}$$

where ρ is the mass density, λ, μ the Lamé constants, δ_{ij} the Kronecker delta and $H(\ )$ the Heaviside function. The fundamental singular solution for the tractions F_{ij} is

$$F_{ij} = \frac{\mu}{2\pi\rho}\left\{\frac{1}{c_1}H(c_1t'-r)\left[\frac{A_1}{A_1^3}+(2c_1t'-r)\frac{2A_2}{R_1r^3}\right]\right.$$
$$\left.-\frac{1}{c_2}H(c_2t'-r)\left[\frac{A_3}{R_2^3}+(2c_2t'-r)\frac{2A_2}{R_2r^3}\right]\right\} \tag{37}$$

where

$$A_1 = \left(\frac{\lambda}{\mu}\right) n_i r_j + 2\frac{r_i r_j}{r}\frac{\partial r}{\partial n} \tag{38}$$

$$A_2 = n_i r_j + n_j r_i + \frac{\partial r}{\partial n}\left(r\delta_{ij} - 4\frac{r_i r_j}{r}\right) \tag{39}$$

$$A_3 = \frac{\partial r}{\partial n}\left(2\frac{r_i r_j}{r} - r\delta_{ij}\right) - n_j r_i \tag{40}$$

and $n = \{n_1, n_2\}$ is the vector normal to the boundary Γ^B.

REFERENCES

1. H. Abouseeda and P. Dakoulas, 'Response of earth dams to P and SV waves using coupled FE-BE formulation', *J. Earthquake Engng. Struct. Dyn.* **25**, 1177–1194 (1996).
2. H. Abouseeda and P. Dakoulas, 'Nonlinear dynamic earth dam–foundation interaction', *Proc. 11th World Conf. on Earthquake Engineering*, Acapulćo, Mexico, 1996.
3. A. K. Chopra, M. Dibaj, R. W. Clough, J. Penzien and H. B. Seed, 'Earthquake analysis of earth dams', *Proc. 4th World Conf. on Earthquake Enginering*, Santiago, 1969.
4. P. Dakoulas and G. Gazetas, 'A class of inhomogeneous shear models for seismic response of dams and embankments', *Soil Dyn. Earthquake, Engng.* **4**, 166–182 (1985).
5. P. Dakoulas and C. Hsu, 'Lateral response of earth dams in semi-elliptical rigid canyons', *J. Soil Dyn. Earthquake Engng.* **12**, 497–507 (1994).
6. P. Dakoulas and H. Abouseeda, 'Response of earth dams to Rayleigh waves using coupled FE-BE formulation', *J. Engng. Mech. ASCE* **23**, 1311–1320 (1997).
7. P. Dakoulas and C. Hsu, 'Response of earth dams in semi-elliptical flexible canyons to oblique SH waves', *J. Engng. Mech. ASCE* **121**, 379–391 (1995).
8. P. Dakoulas, 'Response of earth dams in semi-cylindrical valleys subjected to plane SH waves', *J. Engng. Mech. ASCE* **119**, 74–90 (1993).
9. P. Dakoulas, 'Earth dam–canyon interaction effects for obliquely incident SH waves', *J. Geotech. Engng. Div. ASCE* **119**, 1696–1716 (1993).
10. P. Dakoulas and H. Hashmi, 'Wave passage effects on the response of earth dams', *J. Soils Foundations* **32**, 97–110 (1992).
11. A.-W. M. Elgamal, A. M. Abdel-Ghaffar and J. H. Prevost, 'Elastoplastic seismic shear response of 3-D Earth Dams: Application', *J. Geot. Engng. Div. ASCE* **113**, 1309–1325 (1987).
12. A.-W. M. Elgamal, 'Three-dimensional seismic analysis of La Villita Dam', *J. Geotech. Engng. ASCE* **118**, 1937–1958 (1992).
13. L. W. D. Finn, R. H. Ledbetter and W. F. Marcuson III, 'The evolution of Geotechnical Earthquake Engineering Particle in North America: 1954–1994', *Proc. 3rd Int. Conf. on Recent Advances in Geotech. Earthquake Engineering and Soil Dynamics*, St. Louis, Mo, Vol. 2, 1995, pp. 881–909.
14. G. Gazetas. 'Seismic response of earth dams: some recent developments', *J. Soil Dyn. Earthquake Engng.* **6**(1), 1–47 (1987).
15. G. Gazetas and P. Dakoulas, 'Seismic analysis and design of rockfill dams: state-of-the art', *J. Soil Dyn. Earthquake Engng.* **11**, 27–61 (1992).
16. G. Gazetas and N. Uddin, 'Permanent deformation on preexisting sliding surfaces in dams', *J. Geotech. Engng ASCE* **120**, 2041–2061 (1994).
17. G. Gazetas, 'Shear vibration of veritically inhomogeneous earth dams', *Int. J. Numer. Anal. Meth. Geomech.* **6**, 219–241 (1982).
18. F. I. Makdisi and H. B. Seed, 'Simplified procedure for estimating dam and embankment response', *J. Geotech. Engng. Div. ASCE* **104**(7), 849–867 (1978).
19. W. F. Marcuson III, M. E. Hynes, A. G. Franklin, 'Seismic stability and deformation analysis: the last twenty five years', *Geotech. Special Publication No. 31*, ASCE, Vol. 1, 1992, pp. 552–592.
20. L. H. Mejia and H. B. Seed and J. Lysmer, 'Dynamic analysis of earth dams in three dimensions', *J. Geotech. Engng Deivision, ASCE* **108**, 1586–1604 (1982).
21. H. B. Seed, 'Considerations in the earthquake resistant design of earth and rockfill dams'. *Geotechnique* **29**, 215–263 (1979).
22. J. H. Prevost, A. M. Abdel-Ghaffar, A. W. M. Elgamal 'Nonlinear hysteretic response of soil systems', *J. Engng. Mech. ASCE* **111**, 882–897 (1985).
23. D. V. Griffiths and J. H. Prevost, 'Two- and three-dimensional dynamic finite element analyses of the Long Valley Dam', *Geotechnique* **38**, 367–388 (1988).
24. A. Yiangos and J. H. Prevost, 'Two-dimensional two-phase elasto-plastic seismic response of earth-dams', *Research Rep. NCEER*, State Univ. of New York, Buffalo, 1991.
25. L. W. D. Finn, 'Dynamic Analysis in Geotechnical Engineering', *Proc., Earthquake Engineering and Soil Dynamics II—Recent Advances in Ground Motion Evaluation*, ASCE, 1988, pp. 523–591.

26. L. W. D. Finn, M. Yogendrakumar, N. Yoshida and H. Yoshida, 'TARA-3: A progran to compute the response of 2-D embankments and soil–structure systems to seismic loadings', Dept. of Civil Engineering, University of British Columbia, Canada 1986, *Unpublished Report, proprietory use*.
27. O. C. Zienkiewicz, M. Pastor and C. Chan, and Y. Xie, 'Computational approaches to the dynamics and statics of saturated and unsaturated soils', *Advanced Geotechnical Analyses*, Develop. in Soil Mech. and Found. Engin. Vol. 4, Banerjee, P. K. and Butterfield, R. (eds), Elsevier, Amsterdam, 1991, pp. 151–190.
28. Z. P. Liao and H. L. Wong, 'A transmitting boundary for the numerical simulation of elastic wave propagation', *Soil Dyn. Earthquake Engng.* **3**, 174–183 (1984).
29. E. Kausel, 'Local transmitting boundaries', *J. Engng. Mech. ASCE* **114**, 1011–1027 (1988).
30. E. Kausel and J. T. Tassoulas, 'Transmitting boundaries: a closed-form comparison', *Bull. Seism. Soc. Am.* **71**, 143–159 (1981).
31. C. Zhao, S. Valliapan and Y. C. Wang, 'A numerical model for wave scattering problems in infinite media due to P and SV wave incidences', *Int. J. Numer. Meth. Engng* **33**, 1661–1682 (1992).
32. C. Zhao and S. Valliappan, 'Seismic wave scattering effects under different canyon topographic and geological conditions', *J. Soil Dyn. Earthquake Engng.* **12**, 129–143 (1993).
33. D. E. Beskos, 'Boundary element methods in dynamic analysis', *Appl. Mech. Rev.* **40**, 1–23 (1987).
34. S. Ahmad and P. K. Banerjee, 'Multi-domain BEM for two-dimensional problems of elastodynamics', *Int. J. Num. Meth. Engng* **26**, 891–911 (1988).
35. O. C. Zienkiewicz, D. M. Kelly and P. Bettes, 'The coupling of the finite element method and the boundary solution procedures', *Int. J. Numer. Meth. Engng* **11**, 355–376 (1977).
36. C. A. Brebbia, J. C. F. Telles and L. C. Wrobel, *Boundary Element Techniques*, Springer, Berlin, Heidelberg, New York, 1984.
37. O. von Estorff and E. Kausel, 'Coupling of boundary and finite elements for soil–structure interaction problems', *Earthquake Engng Struct. Dyn.* **18**, 1065–1075 (1989).
38. C. C. Spyrakos and D. E. Beskos, 'Dynamic response of flexible strip-foundations by boundary and finite elements', *Soil Dyn. Earthquake Engng* **5**, 84–96 (1986).
39. O. von Estorff and M. J. Prabucki, 'Dynamic response in the time domain by coupled boundary and finite elements', *Comput. Mech.* **9**, 35–46 (1990).
40. T. Touhei and T. Ohmachi, 'Modal analysis of a dam–foundation system based on a FE–BE method in the time domain, *Earthquake Engng. Struct. Dyn.* **23**, 1–15 (1994).
41. T. Touhei and T. Ohmachi, 'A FE–BE method for dynamic analysis of dam–foundation–reservoir systems in the time domain', *Earthquake Engng. Struct. Dyn.* **22**, 195–209 (1993).
42. G. D. Pavlatos and D. E. Beskos, 'Dynamic elastoplastic analysis by BEM/FEM', Engineering Analysis with Boundary Elements, **14**, 51–63 (1994).
43. G. D. Pavlatos and D. E. Beskos, 'Dynamic inelastic soil–structure interaction using a hybrid BEM/FEM scheme', *Proc. IUTAM/IACM Symp. on Discretization methods in Structural Mechanics* II, Viena 2–6 June, 1997.
44. S. Valliappan and M. Yazdchi, 'Seismic response of concrete gravity dams—A continuum damage mechanics approach', *Proc. IUTAM/IACM Symp. on Discretization methods in Structural Mechanics II*, Viena 2–6 June 1997.
45. A. C. Eringen and E. S. Suhubi, *Elastodynamics*, Academic Press, New York, 1975.
46. O. C. Zienkiewicz, *The Finite Element Method*, 3rd edn., McGraw-Hill, New York, 1977.
47. H. Antes, 'A boundary element procedure for transient wave propagation in two-dimensional isotropic elastic media', *Finite Element Anal. Des.* **1**, 313–322 (1985).
48. T. A. Cruse and F. J. Rizzo, 'A direct formulation and numerical solution of the general transient elastodynamic problem 1', *Int. J. Math. Anal. Appl.* **22**, 244–259 (1968).
49. W. J. Mansur and C. A. Brebbia, 'Formulation of the boundary element method for transient problems governed by the scalar wave equation', *Appl. Math. Modelling* **6**, 307–311 (1982).
50. H. D. Hibbit, B. I. Karlsson and E. P. Sorensen, Inc., *ABAQUS, General-purpose Finite Element Program*, Providence, RI, 1995.
51. H. Antes and P. D. Panagiotopoulos, *The Boundary Integral Approach to Static and Dynamic Contact Problems*, Birkhäuser Verlag, Boston, 1992.
52. P. K. Banerjee, *The Boundary Element Methods in Engineering*, McGraw Hill, New York, 1994.
53. D. P. Henry and P. K. Banerjee, 'A variable stiffness type boundary element formulation for axisymmetric elastoplastic media', *Int. J. Numer. Meth. Engng* **26**, 1005–1027 (1988).
54. I. M. Idriss, J. M. Mathour and H. B. Seed, 'Earth dam–foundation interaction during earthquakes', *J. Earthquake Engng. and Struct. Dyn.* **2**, 313–323 (1974).
55. D. L. Karabalis and D. E. Beskos, 'Dynamic response of 3-D flexible foundations by time domain BEM and FEM', *Soil Dyn. Earthquake Engng.* **4**, 91–101 (1985).
56. T. K. Mossessian and M. Dravinski, 'Application of hybrid method for scattering of P, SV, and Rayleigh waves by near-surface irregularities', *Bull. Seism. Soc. Am.* **77**, 1784–1803 (1987).
57. J. L. Tassoulas, 'Dynamic soil–structure interaction', in *Boundary Element Methods in Structural Analysis.* D. E. Beskos (ed.), Am. Society of Civil Engineers, New York, 1988.
58. O. von Estorff and H. Antes, 'On FEM-BEM coupling for fluid–structure interaction analysis in time domain', *Int. J. Numer. Meth. Engng* **31**, 1151–1168 (1991).
59. J. Wolf, *Dynamic Soil–structure Interaction*, Prentice-Hall, Englewood Cliffs, NJ (1985).

